Production of cold CN molecules by photodissociating ICN precursors in brute-force field*

Wen-Xia Xu(徐文霞), Yong-Cheng Yang(杨永成), and Lian-Zhong Deng(邓联忠)†

State Key Laboratory of Precision Spectroscopy, East China Normal University, Shanghai 200062, *China*

(Received 22 December 2016; revised manuscript received 22 February 2017; published online 30 March 2017)

We theoretically investigate the production of cold CN molecules by photodissociating ICN precursors in a brute-force field. The energy shifts and adiabatic orientation of the rotational ICN precursors are first investigated as a function of the external field strength. The dynamical photofragmentation of ICN precursors is numerically simulated for cases with and without orienting field. The CN products are compared in terms of their velocity distributions. A small portion of the CN fragments are recoiled to near zero speed in the lab frame by appropriately selecting the photo energy for dissociation. With a precursor ICN molecular beam of ~ 1.5 K in rotational temperature, the production of low speed CN fragments can be improved by more than 5 times when an orienting electrical field of 100 kV/cm is present. The corresponding production rate for decelerated fragments with speeds ≤ 50 m/s is simulated to be about $\sim 2.1\times10^{-4}$ and CN number densities of 10^{8}–10^{10} cm^{-3} can be reached with precursor ICN densities of $\sim 10^{12}$–10^{14} cm^{-3} from supersonic expansion.

Keywords: cold molecules, photodissociation, molecular orientation

PACS: 37.10.Mn, 37.90.+j, 33.80.Gj **DOI:** 10.1088/1674-1056/26/5/053702

1. Introduction

Over the past few decades, cold atoms and molecules have been actively pursued for their applications in a wide range of research areas, like high-resolution spectroscopy, cold collisions, precision measurement, many-body physics, quantum information science, cold chemistry, etc. Compared to cold atoms, cold molecules with both richer internal structures and chemical properties have inspired even stronger interest among researchers. A variety of techniques have been developed for the production of cold molecules, like buffer gas cooling,[1] Stark deceleration,[2] and laser cooling.[3–5] Ultracold molecules photoassociated from laser cooled atoms have also been reported.[6–9] Continuing efforts in search of new methods for the production of cold atoms and molecules have never ceased.[10–17] In 2007, Matthews *et al.*[18] proposed that cold oxygen atoms could be made with zero mean velocity in the laboratory frame by photodissociating NO_2 molecules.

Later, this method was demonstrated in an experiment producing slow NO molecules[19] and was given the name of photostop.[20] Cold bromine (Br) atoms near zero velocity were also obtained[21] by photodissociating Br_2 precursors and even trapped with a magnetic field.[22] The means toward improving the production efficiency for cold atoms of low velocities during photodissociation were also proposed and theoretically investigated.[23,24]

The cyano radical (CN) is one of the first detected molecules in the interstellar medium and has also been found extensively in many other systems, like atmospheric carbon arcs and low pressure discharges. It is widely involved in the creation and destruction of various cyanides, most of which are notoriously toxic. The availability of a cold CN sample will help us to better understand the hyperfine structure of this triple-valence-bond molecule and investigate its physical and chemical properties.

In this paper, we carry out a theoretical study on the production of cold CN radicals by photodissociating ICN precursors brute-force oriented in an electrostatic field. The energy shifts of the rotational ICN molecules exposed to the orienting electrical field are first studied using the matrix method. The dependence on the electrical field strength of the adiabatic orientation of the ICN dipole is also investigated. The fragmentation processes of ICN precursors with and without the orienting field are then numerically simulated using the Monty–Carlo method. The recoiled CN molecules are compared for both cases in terms of their velocity distributions. Some discussion and a conclusion are given in the end.

2. ICN molecules exposed to orienting electrical field

For manipulation of molecules with electric (or magnetic) fields, a detailed understanding of the influence of the external field on the energy levels of the molecule is helpful. The field-dependent eigenstate of the molecule can be expressed as a linear combination of its field-free eigenstates. These field-free quantum states are used as a set of basis vectors, upon which the field-dependent Hamiltonian matrix of the molecule is composed. The eigenvalues of the field-dependent eigenstates can be found from the elements along the principle diag-

*Project supported by the National Natural Science Foundation of China (Grant Nos. 11504112, 91536218, and 11604100).

†Corresponding author. E-mail: lzdeng@phy.ecnu.edu.cn

© 2017 Chinese Physical Society and IOP Publishing Ltd

onal axis of the matrix after diagonalization. The projections of the field-dependent eigenstates on the basis vectors, i.e., the coefficients, can also be obtained from the accompanying matrix for diaganolization. This is the basic idea underlying the numeric matrix method.[25] In practice, the number of the selected basis vectors should be large enough to ensure accuracy of the solution but not too large to save expenditure on computing time.

The electronic ground state ICN molecule is linear in geometry and has an electric dipole moment of 3.8 D.[26] Upon rigid rotor approximation, the field-dependent Hamiltonian for the rotational ICN molecule can be expressed as $H = BJ(J+1) + W_{\text{Stark}}$. Here $W_{\text{Stark}} = -\boldsymbol{\mu}\cdot\boldsymbol{E}$ is the interaction between the electrical field $\boldsymbol{E}$ and the electric dipole $\boldsymbol{\mu}$ of the molecule, J is the rotational quantum number, and B is the rotational constant of the molecule. In the absence of electrical field (E-field), the eigenstates of the rotational ICN molecule are labeled as $|JM\rangle$. With the presence of the external E-field, the corresponding eigenstate can be expressed as $|\tilde{J},M\rangle = \sum_{J'>|M|} C_{J'}^{JM}|J',M\rangle$, since only quantum states of the same M are coupled. Using the above-mentioned numeric matrix method, the rotational energy of the ICN molecule can be conveniently obtained. Figure 1 shows the Stark energy shifts of the ICN molecule as a function of the E-field strength for some rotational levels ($J = 0$, 1, 2, and 3). When the E-field is not strong, there are both low-field-seeking (positive energy shift, $\boldsymbol{\mu}//-\boldsymbol{E}$) and high-field-seeking (negative energy shift, $\boldsymbol{\mu}//\boldsymbol{E}$) quantum states for the rotational molecule. As the E-field increases, the molecule, irrespective of its quantum state, will finally turn into a strong-field seeker (negative energy shift, $\boldsymbol{\mu}//\boldsymbol{E}$).

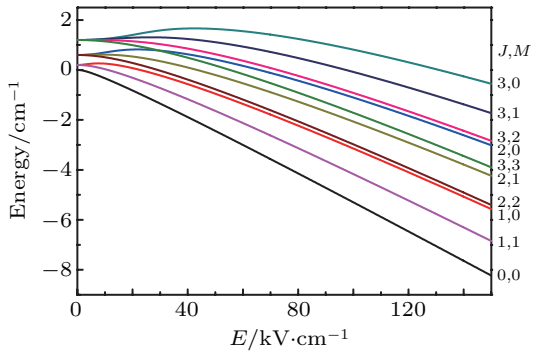


Fig. 1. (color online) The rotational energy levels ($J = 0$, 1, 2, 3) of the ICN molecule ($B = \sim 0.092$ cm^{-1}) in the vibronic ground state as a function of the E-field strength.

The orientation of a linear molecule can be characterized by its orientational probability distribution function (OPDF), which indicates the distribution of the molecular axis orientation with respect to the direction of the external E-field. According to the literature,[27] the field dependent OPDF of the rotational ICN molecule, $P_{JM}(\cos\theta, E)$, can be written as

$$\begin{aligned} & P_{JM}(\cos\theta, E) \\ &= \int |\Phi_{JM}|^2 = \int_0^{2\pi} \mathrm{d}\varphi \int_0^{2\pi} \mathrm{d}\chi \Phi_{JM}(E)^* \Phi_{JM}(E) \\ &= \sum_{J',J''} c_{J'}^{JM} c_{J''}^{JM} \frac{(2J'+1)^{1/2}(2J''+1)^{1/2}}{2}(-1)^M \\ &\quad \times \sum_{n=|J'-J''|}^{J'+J''} (2n+1) \\ &\quad \times \begin{pmatrix} J' & J'' & n \\ M & -M & 0 \end{pmatrix} \times \begin{pmatrix} J' & J'' & n \\ 0 & 0 & 0 \end{pmatrix} \times P_n(\cos\theta). \end{aligned} \tag{1}$$

Here $\Phi_{JM}(E) = |\tilde{J}M\rangle = \sum_{J'} C_{J'}^{JM}|J'M\rangle$ is the wave function of the field-dependent eigenstate of the molecule, $P_n(\cos\theta)$ is the n-th order Legendre polynomial, and the two elements before $P_n(\cos\theta)$ are conventional 3-j symbols. Substituting into Eq. (1) the field-dependent eigenstate vector calculated above using the matrix method, one can obtain the degree of orientation for the state, $\langle\cos\theta\rangle = \langle\tilde{J},M|\cos\theta|\tilde{J},M\rangle$. Figure 2 shows $\langle\cos\theta\rangle$ as a function of the E-field strength for a few rotational states of ICN. Due to its small rotational constant and big electric dipole moment, ICN of the lowest rotational states can be well oriented under an E-field of strength ~ 100 kV/cm, which is readily available for normal experimental conditions. As the energy of the rotating molecule gets higher with increasing J, it becomes less tame to the orienting E-field, as shown by the various curves. The change of $\langle\cos\theta\rangle$ in sign (from negative to positive values) indicates the transition of the molecular orientation (from being anti-parallel to parallel), as can be seen from curves for states like $|J,M\rangle = |1,0\rangle$, $|2,0\rangle$, and $|2,1\rangle$.

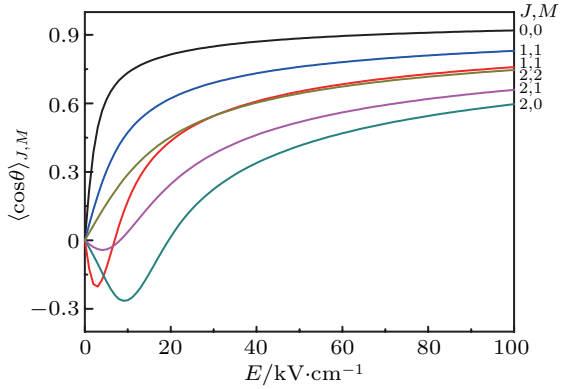


Fig. 2. (color online) The degree of orientation, $\langle\tilde{J},M|\cos\theta|\tilde{J},M\rangle$, of the ICN molecule as a function of the E-field strength for states of $J = 0$, 1, and 2.

For a molecule ensemble of rotational temperature T_{rot}, the value of $\langle\cos\theta\rangle$ needs to be further averaged over all the quantum states populated according to their respective thermal statistical weight $P(\tilde{J},M)$ and is given as

$$\langle\langle\cos\theta\rangle\rangle = \sum_{JM} P(\tilde{J},M)\langle\cos\theta\rangle_{\tilde{J}M}. \tag{2}$$

Here $P(\tilde{J},M)$ is governed by the Boltzmann distribution law and given by

$$P(J,M) = \frac{1}{Z}\exp-\left(\frac{BJ(J+1)}{kT_{\rm rot}}\right), \tag{3}$$

with the partition function given by

$$Z = \sum(2J+1)\exp[-(BJ(J+1)/kT_{\rm rot})].$$

Therefore, the degree of orientation of a molecule ensemble has a strong dependence on its rotational temperature $T_{\rm rot}$.

3. Photostop of CN molecules from ICN precursors

3.1. Overeview

The photodissociation dynamics of ICN in the A continuum has been extensively investigated.[28–39] Photodissociation of brute-force oriented ICN has also been experimentally reported.[40,41] It has been well established through experimental and theoretical studies that there are two possible dissociation channels in the medium energy region (290–248 nm) of the A continuum:

$$\begin{aligned}&{\rm ICN}\rightarrow{\rm ICN}^{*}\rightarrow{\rm I}(^{2}{\rm P}_{3/2})+{\rm CN}(\mathrm{X}^{2}\Sigma^{+})\\&\rightarrow{\rm I}^{*}(^{2}{\rm P}_{1/2})+{\rm CN}(\mathrm{X}^{2}\Sigma^{+}).\end{aligned} \tag{4}$$

The first channel leads to an iodine atom ($\mathrm{I}^{2}\mathrm{P}_{3/2}$) and a CN radical of the ground state ($\mathrm{CN}^{2}\Sigma^{+}$); while the second channel leads to a molecule of the ground state ($\mathrm{CN}^{2}\Sigma^{+}$) and an atom of the spin–orbit excited state ($\mathrm{I}^{*2}\mathrm{P}_{1/2}$). Three main potential surfaces have been found to contribute in the A continuum.[33] The parallel transition to the $^{3}\Pi_{0+}$ surface is the major component, while the perpendicular transitions to $^{1}\Pi_{1}$ and $^{3}\Pi_{1}$ surfaces are thought to contribute more in the blue and red wings of the absorption curve. ICN molecules excited to the $^{3}\Pi_{0+}$ surface are almost linear in geometry along the dissociation coordinate and adiabatically correlate to the I^{*} products, leading mainly to CN fragments of low rotation. ICN molecules excited to the $^{1}\Pi_{1}$ and $^{3}\Pi_{1}$ surfaces, however, have a strong preference for bending and adiabatically correlate to the I products, leading mainly to rotationally excited CN fragments. The resulting CN fragments primarily populate the vibronic ground state.[38]

The basic idea of photostopping a CN molecule from an ICN precursor is as follows: a precursor ICN molecule moves with velocity $v_{\rm ICN}$ in the lab frame. After absorption of a photon, the ICN dissociates into a CN radical and an I atom. The I atom is recoiled forward and gets accelerated, while the CN radical is recoiled backward and gets decelerated. The energy of the photon is chosen so that the recoil velocity of the CN, $u_{\rm CN}$, just cancels its original velocity $v_{\rm ICN}$, and the CN is brought (i.e., photostopped) to a standstill in the lab frame. More details about the kinematics of the photostop process can be found in Refs. [20] and [23].

Energy conservation for the system under consideration in the center of mass (COM) frame can be expressed as

$$E(h\nu)+E_{\rm int}({\rm ICN})-D_{0}=E_{\rm SO}+E_{\rm int}({\rm CN})+E_{\rm T}, \tag{5}$$

where $E(h\nu)$ is the photon energy, $E_{\rm int}(\mathrm{ICN})$ is the internal energy of ICN, D_0 is the dissociation energy of the I–CN bond ($\sim 26980\ \mathrm{cm}^{-1}$), $E_{\rm SO}$ is the spin–orbit energy of the iodine atom ($0\ \mathrm{cm}^{-1}$ for I and $7603\ \mathrm{cm}^{-1}$ for I^{*}), $E_{\rm int}(\mathrm{CN})$ is the internal energy of the CN fragment, and $E_{\rm T}=E_{\rm T}(\mathrm{I})+E_{\rm T}(\mathrm{CN})$ is the kinetic energy available to both fragments. From conservation of energy and momentum, the recoil velocity of the CN in the COM frame is given as

$$u_{\rm CN}=\sqrt{2E_{\rm T}\frac{M_{\rm I}}{M_{\rm CN}(M_{\rm I}+M_{\rm CN})}}, \tag{6}$$

with $M_{\rm I}$ and $M_{\rm CN}$ being the masses of the I atom and CN molecule, respectively.

3.2. Numerical simulation

In fact, due to the finite angular distribution of the fragmentation,[42] the velocity distribution of the recoiled CN fragments is rather broad, even though a polarized laser for dissociation has been adopted. Only a small portion of the CN molecules are lucky enough to have their original kinetic energy almost canceled during the recoil and have velocities near zero. These lucky ones are mostly CN fragments who recoil backward parallel to or only in small angles with respect to the precursor beam axis. Orientation of the precursor ICN molecules with a brute-force E-field along the molecular beam axis will greatly improve the probability of fragmentation along this direction, and thus the production rate of CN fragments near zero velocity.

The fragmentation of $\mathrm{I}^{127}\mathrm{C}^{12}\mathrm{N}^{14}$ precursors to produce slow CN radicals is simulated using the Monte–Carlo method for cases with and without orienting E-field. The ICN molecular beam for simulation has its longitudinal velocity (v_z) centered at 560 m/s with a FWHM spread of 50 m/s and its transverse velocities (v_x and v_y) centered at zero with a FWHM spread of 10 m/s. Such a precursor beam is readily obtained by supersonically expanding ICN molecules seeded in argon (Ar) gases. The rotational temperature of the ICN beam is taken to be ~ 1.5 K.[41] The electrical field $\boldsymbol{E}$ for precursor orientation and the polarization of the laser field for photodissociation are both along the molecular beam axis (i.e., the z direction). Both product channels, as mentioned in Eq. (4), are considered during simulations. The wavelength of the dissociation laser is chosen to be ~ 285 nm so that the photon energy requirement for photostopped CN from the second channel is met, since we are more interested in cold CN radicals of low rotation. The quantum yield of I^{*} from ICN at a dissociation wavelength of

$\sim$ 284 nm was experimentally studied to be about $\sim$ 53%[31] and an estimated value of $\sim$ 50% is taken here for $\sim$ 285 nm dissociation. According to the literature,[29,31] the average rotational energy of the CN molecules from the I* channel of our interest is estimated as $\sim$ 75 cm^{-1}.

Figure 3 shows the velocity distributions of the ground state ($^2\Sigma^+$) CN molecules after photostop in the z direction and x (or y) direction, respectively. The results presented are for cases with the orienting E-field being 0 kV/cm and 100 kV/cm, respectively. CN molecules resulted from both product channels are discernible in the plot for the case of $E = 0$ kV/cm. The central high peaks correspond to CN molecules from the I* channel. Those molecules which appear near the zero velocity are successfully photostopped and in our pursuit. The CN molecules from the I channel share more kinetic energy and have much higher velocities. They contribute mainly to the outside low peaks (or shoulders). Without orienting field, the CN product has a fifty-to-fifty probability of being accelerated or decelerated. With an orienting E-field of $\sim$ 100 kV/cm along the positive z direction, almost all ICN precursors in the molecular beam ($T_{\rm rot} = 1.5$ K) are turning into strong-field seekers (see Fig. 2) with the CN part being oriented to some extent toward the negative z direction. After fragmentation, almost all CN fragments are recoiled backward and more of them can be well photostopped, as shown by the increased height of the peak near zero velocity in Fig. 3.

To have a quantitative idea of the improvement on the production of the decelerated fragments by the orienting E-field, let us examine the total speed (i.e., $v = \sqrt{v_x^2 + v_y^2 + v_z^2}$) distribution of the CN molecules, as shown in Fig. 4 with a log–linear scale. The number of molecules is statistically counted as a function of the speed with an interval of 10 m/s. The maximum speed is truncated at $\sim$ 750 m/s just for viewing purposes. The open squares and circles correspond to cases of $E = 0$ kV/cm and 100 kV/cm, respectively. The solid squares indicate the initial speed distribution of the ICN precursors in the supersonic beam. The number of CN molecules is normalized to that of the most probable speed in the ICN precursor beam. For instance, the relative numbers of CN at speeds of $v = 10$ m/s, 50 m/s, and 100 m/s are counted to be $\sim 1.65 \times 10^{-5}$, $\sim 9.65 \times 10^{-4}$, and $\sim 2.82 \times 10^{-3}$ for the case of $E = 0$ kV/cm. These corresponding numbers increase, however, to $\sim 1.05 \times 10^{-4}$, $\sim 4.84 \times 10^{-3}$, and $\sim 1.41 \times 10^{-2}$ for the case of $E = 100$ kV/cm. The improvement factor, defined as the ratio of the number of CN fragments with $E = 100$ kV/cm to that with $E = 0$ kV/cm, is about $\sim$ 6, $\sim$ 5, and $\sim$ 5 for the three velocities of $\sim$ 10 m/s, $\sim$ 50 m/s, and $\sim$ 100 m/s, respectively. This factor gets smaller and smaller as the speed increases, as can be seen in Fig. 4.

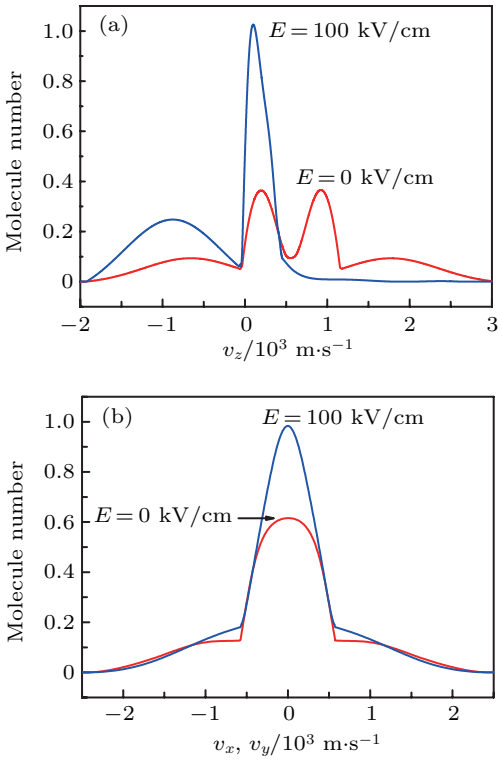


Fig. 3. (color online) The velocity distributions of the ground state ($^2\Sigma^+$) CN molecules after photostop in the z direction (a) and x or y direction (b). The initial temperature T of the ICN precursor beam is $\sim$ 1.5 K. The E-field strength for precursor orientation is marked on the plot.

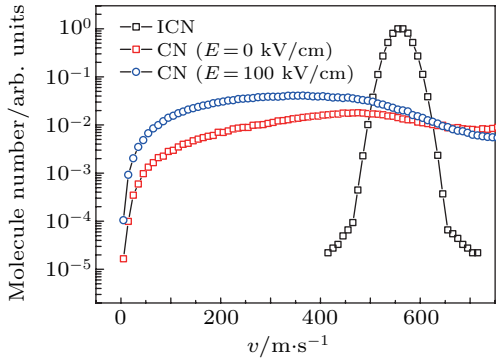


Fig. 4. (color online) The total speed distribution of the CN molecules after photostop. The open squares and circles correspond to cases of $E = 0$ kV/cm and 100 kV/cm, respectively. The solid squares indicate the initial speed distribution of the ICN precursors in the supersonic beam.

The production rate of the decelerated fragments is another interesting quantity concerning photostop. The decelerated CN molecules with their speeds below a certain value, called truncated speed $v_{\rm Tr}$, are statistically accumulated. This count of the number of CN molecules starts from zero speed and proceeds toward high speeds with an interval of $\sim$ 10 m/s. The production rate is defined as the ratio of the accumulated number of CN molecules to the total number of ICN precursors being used, and the corresponding results are shown in Fig. 5. The solid squares and circles correspond to cases of $E = 0$ kV/cm and 100 kV/cm, respectively. For the case of $E =$ 100 kV/cm, the production rate is $\sim 2.0 \times 10^{-6}$, $\sim 2.1 \times 10^{-4}$,

and $\sim 1.1\times10^{-3}$ for CN molecules with speeds ≤ 10 m/s, ≤ 50 m/s, and ≤ 100 m/s, respectively. The production rate increases sharply in the low speed region before continuing its gradual growth toward the high speed region. The improvement on the production of decelerated fragments due to orienting E-field can also be seen here.

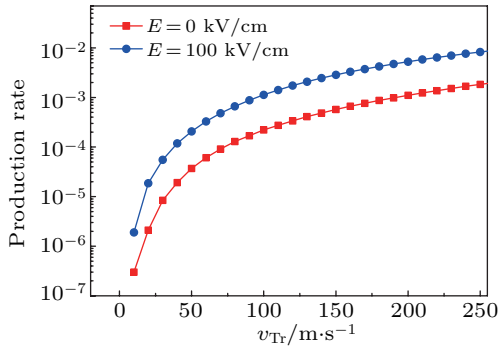


Fig. 5. (color online) The production rate of CN fragments as a function of truncated speed $v_{\rm Tr}$.

4. Discussion and conclusion

In this paper, we have theoretically studied the production of cold CN molecules near zero speed by photodissociating ICN precursors brute-force oriented in an electrical field. The Stark energy shifts of rotational ICN molecules exposed to an orienting electrical field were first studied using the matrix method. The dependence of the adiabatic orientation of the ICN dipoles on the orienting E-field strength was also investigated. Depending on its quantum state, the rotational molecule can orient in parallel or anti-parallel to the direction of the weak E-field. As the E-field increases in strength and gets strong enough, the molecule, irrespective of its quantum state, will finally turn into a strong-field seeker and orient along the direction of the E-field. The photofragmentation of ICN precursors with orienting E-field of ~ 0 kV/cm and ~ 100 kV/cm have been numerically simulated. The recoiled CN fragments were compared for both cases in terms of their velocity distributions. With the presence of the orienting E-field of ~ 100 kV/cm, the number of low-speed ($v \leq 100$ m/s) CN fragments can be improved by about 5 times. The corresponding production rate of photostopped CN fragments ($v \leq 10$ m/s) is on the order of $\sim 10^{-6}$. Precursor molecular beams from supersonic expansion readily have densities of $\sim 10^{12}$–10^{14} cm^{-3}. Thus the photostopped CN molecules ($v \leq 10$ m/s) may have a number densities on the order of $\sim 10^{6}$–10^{8} cm^{-3}. For some applications, molecules with speeds ≤ 50 m/s or even larger might be acceptable, and the number density can be increased to about $\sim 10^{8}$–10^{10} cm^{-3} according to the simulated production rate of $\sim 2.1\times10^{-4}$ above. The total number of target molecules in pursuit also depends upon the volume in which they can be prepared. The single-photon absorption based photostop technique can make full use of the big volume available in supersonic precursor beams (especially in the propagation direction) with little worry about the required laser energy for dissociation. In addition, the number of photostopped molecules can also be increased by accumulation from multiple molecular pulses.

References

[1] Maxwell S E, Barhms N, Decarvalho R, Glenn D R, Helton J S, Nguyen S V, Patterson D, Petricka J, Demille D and Doyle J M 2005 *Phys. Rev. Lett.* **95** 173201
[2] Bethlem H L, Berden G and Meijer G 1999 *Phys. Rev. Lett.* **83** 1558
[3] Shuman1 E S, Barry1 J F and DeMille1 D 2010 *Nature* **467** 820
[4] Hummon M T, Yeo M, Stuhl B K, CollopyA L, Xia Y and Ye J 2013 *Phys. Rev. Lett.* **110** 143001
[5] Truppe S, Williams H, Hambach M, Fitch N, Wall T E, Hinds E A, Sauer B E and Tarbutt M R 2017 *New J. Phys.* **19** 022001
[6] Jones K M, Tiesinga E, Lett P D and Julienne P S 2006 *Rev. Mod. Phys.* **78** 483
[7] Kohler T, Goral K and Julienne P S 2006 *Rev. Mod. Phys.* **78** 1311
[8] Ji Z H, Wu J Z, Ma J, Feng Z G, Zhang L J, Zhao Y T, Wang L R, Xiao L T and Jia S T 2010 *Chin. Phys. Lett.* **27** 053701
[9] Ji Z H, Zhang H S, Wu J Z, Yuan J P, Zhao Y T, Ma J, Wang L R, Xiao L T and Jia S T 2011 *Chin. Phys. Lett.* **28** 083701
[10] Friedrich B 2000 *Phys. Rev. A* **61** 025403
[11] Dong G, Lu W and Barker P F 2004 *Phys. Rev. A* **69** 013409
[12] Fulton R, Bishop A I and Barker P F 2004 *Phys. Rev. Lett.* **93** 243004
[13] Hogan S D, Wiederkehr A W, Schmutz H and Merkt F 2008 *Phys. Rev. Lett.* **101** 143001
[14] Yin Y, Zhou Q, Deng L, Xia Y and Yin J 2009 *Opt. Express* **17** 10706
[15] Xia Y, Yin Y L, Ji X and Yin J P 2012 *Chin. Phys. Lett.* **29** 053701
[16] Motsch M, Jansen P, Agner J A, Schmutz H, and Merkt F 2014 *Phys. Rev. A* **89** 043420
[17] Sun H, Wang Z X, Wang Q, Li X J, Liu J P and Yin J P 2015 *Chin. Phys. B* **24** 113101
[18] Matthews S J, Willitsch S and Softley T P 2007 *Phys. Chem. Chem. Phys.* **9** 5656
[19] Zhao B S, Shin S E, Park S, Sun T X and Chung D S 2009 *J. Phys. Soc. Jpn.* **78** 094302
[20] Trottier A, Wrede E and Carty D 2011 *Mol. Phys.* **109** 725
[21] Doherty W G, Bell M T, Softley T P, Rowland A, Wrede E and Carty D 2011 *Phys. Chem. Chem. Phys.* **13** 8441
[22] Rennick C J, Lam J, Doherty W G and Softley T P 2014 *Phys. Rev. Lett.* **112** 023002
[23] Deng L Z and Yin J P 2014 *J. Chem. Phys.* **141** 164314
[24] Bao D X, Deng L Z, Xu L and Yin J P 2015 *Chin. Phys. B* **24** 113702
[25] Hajnal J V and Opat G I 1991 *J. Phys. B* **24** 2799
[26] Li H Z, Franks K J and Kong W 1999 *Chem. Phys. Lett.* **300** 247
[27] Wu M, Bemish R J and Miller R E 1994 *J. Chem. Phys.* **101** 9447
[28] Nadler I, Mahgerefteh D, Reisler H and Wittig C 1985 *J. Chem. Phys.* **82** 3885
[29] Goldfield E M, Houston P L and Ezra G S 1986 *J. Chem. Phys.* **84** 3120
[30] Hall G E, Sivakumar N and Houston P L 1986 *J. Chem. Phys.* **84** 2120
[31] Hess W P and Leone S R 1987 *J. Chem. Phys.* **86** 3773
[32] Kash P W and Butler L J 1992 *J. Chem. Phys.* **96** 8923
[33] Qian J, Tannor D J, Amatatsu Y and Morokuma K 1994 *J. Chem. Phys.* **101** 9597
[34] Guo H and Schatz G C 1990 *J. Chem. Phys.* **92** 1634
[35] Wei H and Carrington T 1996 *J. Chem. Phys.* **105** 141
[36] Wang Y and Qian C X W 1994 *J. Chem. Phys.* **100** 2707
[37] Bowman J M, Mayrhofer R C and Amatatsu Y 1994 *J. Chem. Phys.* **101** 9469
[38] Amatatsu Y, Yabushita S and Morokuma K 1994 *J. Chem. Phys.* **100** 4894
[39] Costen M L, North S W and Hall G E 1999 *J. Chem. Phys.* **111** 6375
[40] Franks K J, Li H, Hanson R J and Kong W 1998 *J. Phys. Chem. A* **102** 7881
[41] Li H, Franks K J and Kong W 1999 *Chem. Phys. Lett.* **300** 247
[42] Chen Y, Yang T and Chen K 2009 *Phys. Chem. Chem. Phys.* **11** 7111